REVIEW ARTICLE
https://doi.org/10.1038/s41929-018-0182-6

nature catalysis

Understanding heterogeneous electrocatalytic carbon dioxide reduction through operando techniques

Albertus D. Handoko[1], Fengxia Wei[1], Jenndy[1,2], Boon Siang Yeo[3] and Zhi Wei Seh[1*]

Renewable energy conversion and storage play an important role in our global efforts to limit the drastic effects of climate change. In particular, the electrocatalytic reduction of carbon dioxide to chemicals and fuels can bring us closer towards a closed-loop anthropogenic carbon cycle. Significant breakthroughs are often the result of deeper understandings of reaction mechanisms, material structures and surface sites. To this end, operando techniques have been invaluable in combining advanced characterization of a catalyst with simultaneous measurements of its activity and selectivity under real working conditions. This Review aims to highlight significant progress in the use of operando characterization techniques that enhance our understanding of heterogeneous electrocatalytic CO_2 reduction. We provide a summary of the most recent mechanistic understanding using operando optical, X-ray and electron-based techniques, along with key questions that need to be addressed. We conclude by offering some insight on emerging directions and prospects in the field.

As of May 2018, 195 member states of the United Nations Framework Convention on Climate Change (UNFCCC) have reached a consensus that climate change represents an urgent and potentially irreversible threat to human societies[1]. The ambitious goals set in the Paris Agreement call for the development of alternative net CO_2 removal strategies beyond the typical options of bioenergy with carbon capture and storage (BECCS) and afforestation[2]. The production of sustainable fuels and feedstock from captured CO_2 and H_2O using renewable energy is considered a viable option[3]. In particular, the electrocatalytic CO_2 reduction reaction (CO_2RR) represents a clean and efficient long-term solution, provided that catalysts with the requisite properties, in terms of activity, selectivity and durability, can be developed[4].

Electrocatalytic CO_2RR is highly complex as it involves the transfer of multiple protons and electrons, together with a number of different possible reaction intermediates and products (Supplementary Tables 1–3 detail relevant equations and standard reduction potential values in acid and base)[5,6]. CO_2RR begins with the adsorption of CO_2 to form $*CO_2$ (or $*CO_2^-$) on the catalyst surface. Various intermediates and products are then formed by step-wise transfer of protons (H^+) and/or electrons (e^-)[6]. Figure 1a presents a possible reaction roadmap that a CO_2 molecule may take during its conversion to various molecules containing one carbon atom (C_1 molecules) via the CO pathway. The grey and red arrows represent transfer of H^+/e^- to the carbon and oxygen sites of the adsorbed molecule, respectively. The blue arrows represent transfer of H^+/e^- to the oxygen site and further removal of a water molecule. Here, we use the CO pathway as a representative example for the formation of C_1 molecules; using the same concept, one can construct other similar reaction routes such as the HCOOH pathway. The reaction pathways to form products with multiple carbon atoms are even more complex, as there are many more permutations to the protonation sites, along with the possible involvement of non-electrochemical steps. Figure 1b shows a possible reaction roadmap for the formation of various molecules containing two carbon atoms (C_2 molecules) via the CO dimerization pathway (Supplementary Note 1 contains more details).

A key requirement for CO_2RR to be commercially viable is the development of proficient catalysts that can achieve both high activity and high selectivity towards valuable products[4]. The common route for catalyst discovery involves long feedback loops of ab initio and kinetics simulation, coupled with experimental and characterization data[7]. Although free energy calculations of adsorbed reaction intermediates have been shown to correlate well with experimental reaction rate and selectivity on simple and well-ordered catalytic systems[8,9], computational screening of new and less ordered catalysts is still challenging, due to the presence of diverse active sites, intermediates and reaction steps[10]. Therefore, researchers worldwide are making a concerted and interdisciplinary effort to apply advanced operando characterization techniques to investigate CO_2RR under real operating conditions. These operando studies can provide important experimental evidence to address five key issues in CO_2RR catalysis: (1) stability of catalyst under reaction condition; (2) identity and configuration of key intermediates; (3) identity of catalytically active sites; (4) preferred reaction pathways and selectivity; and (5) effect of reaction environment.

An illustration of relevant characterization techniques applicable for catalyst materials, along with their known lateral resolution and atomic detection limit range, is presented in Fig. 2. Individually, these characterization techniques can capture minute details of the morphology, size, physical and chemical properties of materials. The real challenge is devising a strategy to allow CO_2RR to take place while satisfying the measurement condition requirements. In this Review, we will highlight significant operando characterization techniques applicable for CO_2RR and how these techniques can help to addresses the five key issues described above. We also identify emerging techniques that have not been demonstrated for CO_2RR,

[1]Institute of Materials Research and Engineering, Agency for Science, Technology and Research (A*STAR), Innovis, Singapore. [2]School of Materials Science and Engineering, Nanyang Technological University, Singapore, Singapore. [3]Department of Chemistry, Faculty of Science, National University of Singapore, Singapore, Singapore. *e-mail: sehzw@imre.a-star.edu.sg

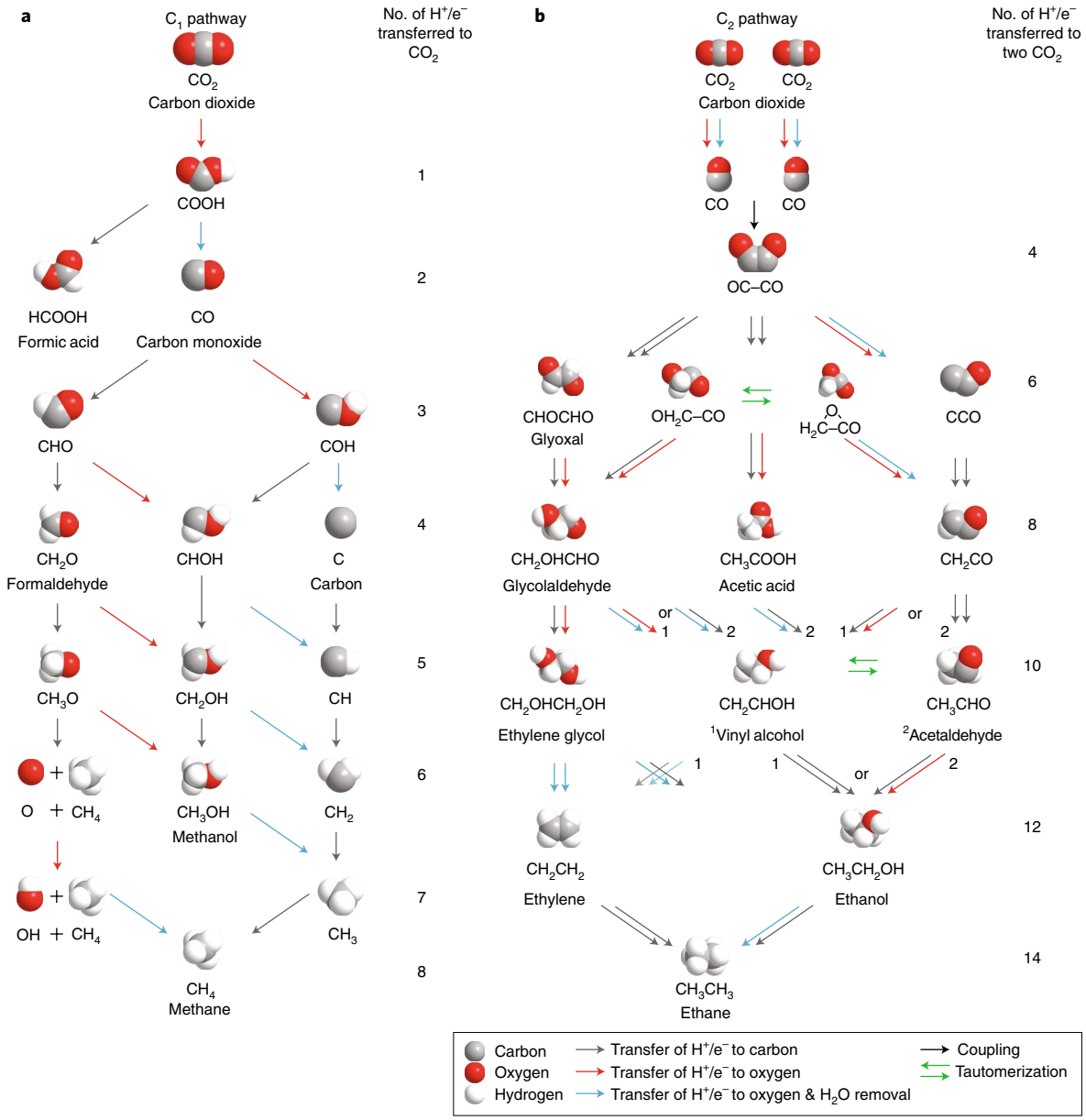

Fig. 1 | Molecular model sketch depicting possible CO_2RR roadmaps to form various C_1 and C_2 products. a,**b**, The pathways towards C_1 products (via CO intermediate; **a**) and C_2 products (via CO dimerization; **b**), organized based on the number of H^+ and e^- pairs transferred. Colour-coded arrows indicate H^+ and e^- transfer to either carbon or oxygen sites as indicated in the legend. Known products are marked with their common name alongside chemical notation. The reaction routes presented here are by no means exhaustive. See Supplementary Note 1 for more details.

but have good potential to provide fresh insight to accelerate CO_2RR catalyst discovery and development.

Optical characterization techniques

Optical spectroscopy includes various techniques utilizing non-ionizing radiation, ranging from the deep ultraviolet to the far infrared. These techniques exploit inelastic light scattering, which can be used to investigate processes such as electron/proton transfer and bond formation at excellent sensitivity and rate. Optical spectroscopy has become the mainstream tool for catalytic investigation, as the wavelength range is relevant to the vibrational frequency of the adsorbed intermediates[11].

Infrared spectroscopy. Taking advantage of the specific absorption of molecular vibrations and the dynamic configuration of the infrared (IR) beam, IR spectroscopy is apt for monitoring adsorbed species on metallic electrode surfaces (as they are likely to contain IR-active modes), but less so for observing catalyst state due to complications in measurements on oxide surfaces[12]. It is a suitable technique to address issues (2), (4) and (5).

Four configurations are accessible to in situ or operando IR spectroscopy measurement of solid samples: transmission, diffuse reflectance, attenuated total reflection (ATR) and reflection–absorption (Fig. 3a–d). As electrocatalytic CO_2RR typically involves submerged and immobilized electrode surfaces, the ATR-IR operating mode is more frequently used as it minimizes the electrolyte layer interference. In this mode, the incoming IR beam is positioned near the critical angle of a specially constructed ATR crystal, such that an evanescent wave formed above the crystal is interacting with adsorbed molecules. The presence of a thin

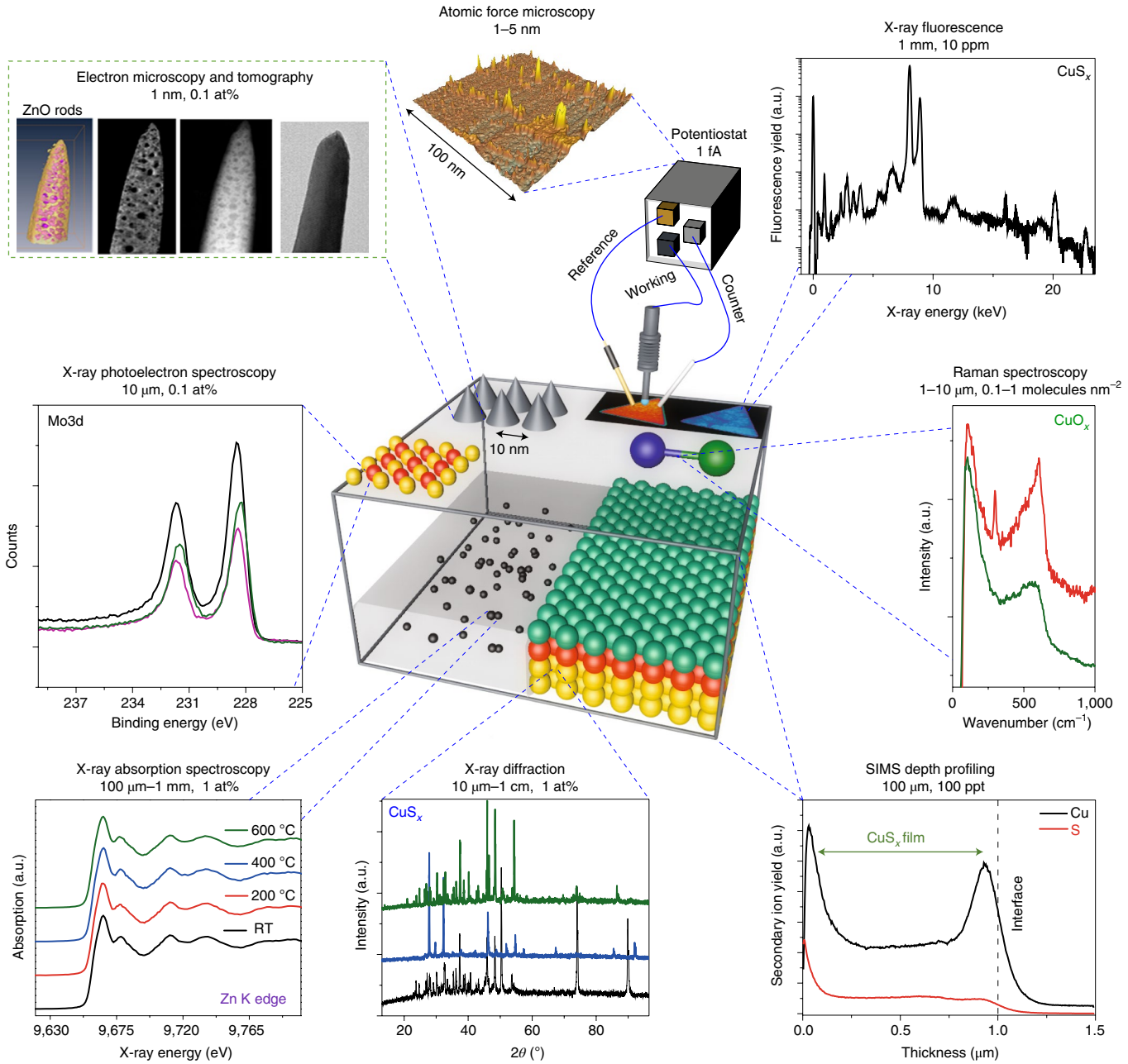

Fig. 2 | Analytical tools commonly applied in the characterization of catalyst materials. Characterization of catalyst materials typically involves multi-faceted ex situ examination using various analytical tools illustrated here to gain insight on their structural, morphological, compositional, chemical and physical properties. A more relevant picture of the catalyst–reactant interaction can be obtained by devising strategies to employ these characterization techniques in real catalytic operando conditions. The typical probe size range and atomic detection limit are indicated. Credit: Electron microscopy and tomography micrographs are adapted from ref. [116], Springer Nature.

metallic layer atop the reflecting crystal plane, also effective as the electrode, enhances the absorption signal due to enhanced electromagnetic field resonance from surface enhancement effects. This technique is often referred to as surface-enhanced infrared absorption spectroscopy (SEIRAS)[13].

SEIRAS is particularly sensitive to adsorbates containing C–O bonds due to their high IR absorption cross-section[11]. In fact, the majority of studies based on operando ATR-SEIRAS on CO_2RR have identified *CO as a common intermediate[14]. However, careful calculation and interpretation is required, as recent operando IR found that bridge-adsorbed *CO is inert to reduction and may not be the sought-after CO_2RR intermediate[15].

Beyond *CO, SEIRAS has been instrumental in demonstrating preferred reaction pathways on various catalysts. For example, a carboxyl intermediate (*COOH) on the surface of a Pt cathode and pyridine redox mediator has been detected under CO_2 purging[16]. Interestingly, the *COOH disappears under CO purging (Fig. 3e), suggesting that *COOH is likely to form through a proton-coupled electron transfer (PCET) step on Pt, distinct from the decoupled steps proposed for Pd surfaces[17]. The presence of *COOH has also been observed on a Ag electrode[18]. However, the appearance of a COO^- symmetric stretch at 1,386 cm^{-1} (Fig. 3g) upon higher overpotential application suggests a mechanism change where the PCET pathway becomes less favourable at this potential.

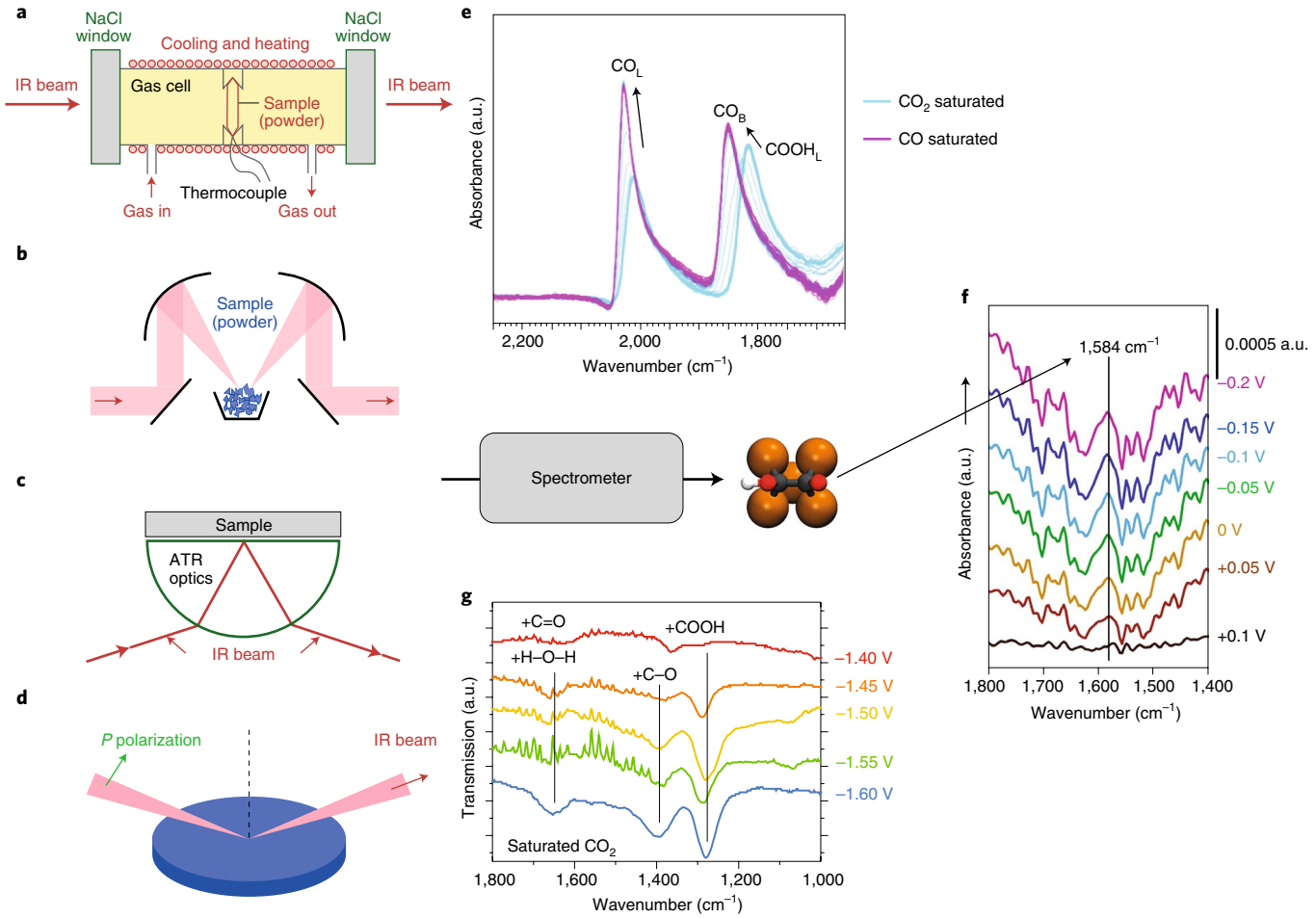

Fig. 3 | IR spectroscopy for operando measurements. a–d, IR spectroscopy is the go-to tool for molecular identification of various sample conditions with four measurement configurations: transmission (**a**), diffuse reflectance (**b**), ATR (**c**) and reflection–absorption (**d**). **e**, More recently, operando IR spectroscopy has enabled the detection of CO_2RR reaction intermediates, specifically change of surface intermediate species from *COOH on CO_2 purging to *CO on CO purging on Pt with pyridine. **f**, Evidence of C–C coupling on $(100)_{Cu}$ in the presence of $^{12}CO_2$ purging in 0.1 M LiOH-D_2O electrolyte. The highlighted band at 1,584 cm^{-1} is assigned to ^{12}C=O stretching of the *OCCOH intermediate. **g**, Rise of the COO^- intermediate at more negative potential on CO_2RR over a Ag catalyst. Credit: Figure adapted from ref. [117], RSC (**a–d**); ref. [16], American Chemical Society (**e**); ref. [28], Wiley (**f**); and ref. [18], American Chemical Society (**g**).

CO_2RR on Sn proceeds slightly differently than with other metals. The observation of monodentate Sn–CO_3 species using SEIRAS on SnO_x electrodes[19] suggests that CO_2RR on SnO_x occurs on partially reduced Sn^{II}-oxy-hydroxide to form a Sn–CO_3 intermediate and finally formate. The presence of partially reduced Sn is also corroborated using Raman spectroscopy[20], which we will discuss further in the next section.

Additionally, SEIRAS also played a central role in uncovering the important role of cations and anions during CO_2RR (issue (5)). Although the influence of ionic species has been investigated[21], only the effect on the potential distribution at the outer Helmholtz plane based on the different cation hydration and local pH was considered. Recently, two separate studies pieced together compelling spectroscopy and isotope-labelling evidence that the majority of CO_2 reactant near the catalyst surface originates from an equilibrium reaction with HCO_3^- (refs [22,23]). The finding is significant, as it changes our perspective on how CO_2 is transported to the catalyst surface, triggering a new wave of theoretical and experimental works to re-examine the role of ions and solvent in CO_2RR (refs [24–27]).

Another significant demonstration of IR spectroscopy for operando CO_2RR is the observation of hydrogenated CO dimers (*OCCOH) on $(100)_{Cu}$ using external reflection configuration (Fig. 3f)[28]. This observation is important as it suggests that the CO–CO dimerization mechanism prevails on $(100)_{Cu}$ surfaces, which leads to high ethylene selectivity[29].

Raman spectroscopy. This method detects the inelastically scattered light due to changes in the rotational or vibrational state of the sample during the scattering event from incoming monochromatic light. As different molecules have varying rotation/vibration states, Raman spectroscopy is sensitive to both the type and configuration of most organic species[30]. In this sense, Raman spectroscopy is complementary to IR spectroscopy and suitable to address issue (2), (4) and (5), but with an added advantage as water has a low Raman scattering cross-section and can be used as the solvent. Additionally, Raman spectroscopy is useful to address issue (3) to some extent as it can monitor the catalyst surface in higher oxidation states.

Widespread use of Raman spectroscopy began when the surface-enhanced Raman scattering (SERS) effect was observed from molecules with weak scattering cross-sections when on top of certain roughened metals[31]. As the inelastic scattering signal must be collected from the illuminated spot, the geometry of an operando

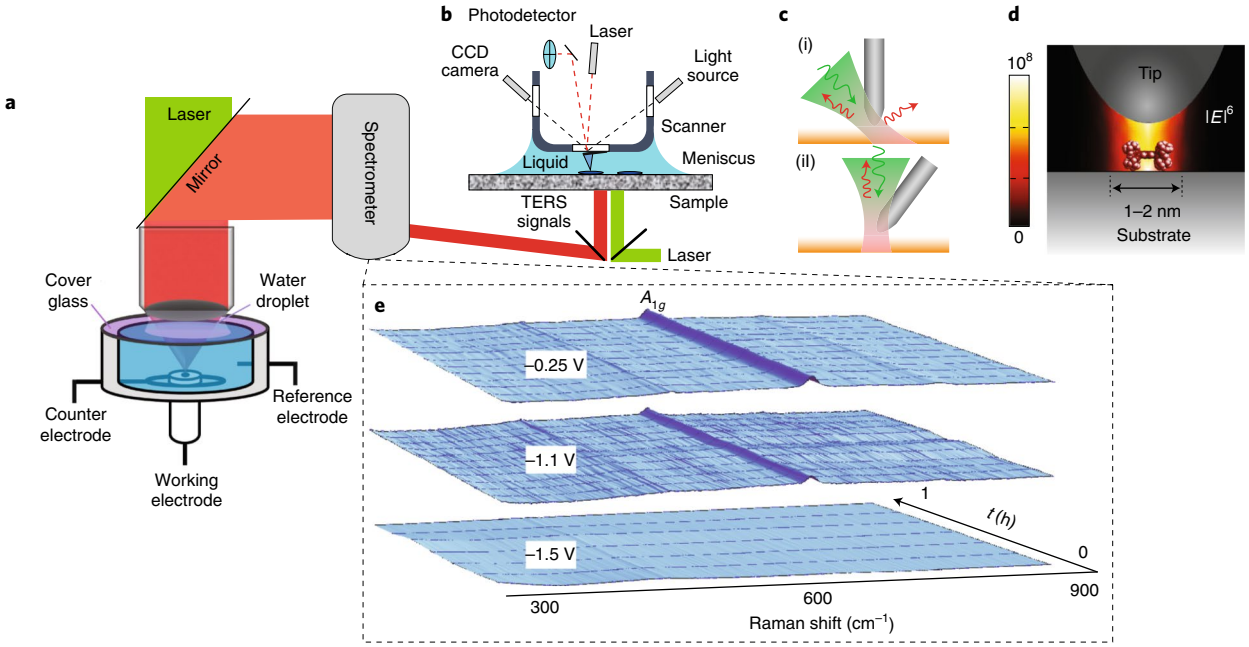

Fig. 4 | Various modifications of Raman spectroscopy setup to enable operando electrochemical measurements and improve detection sensitivity. **a**, Schematics of operando Raman setup with water droplet in between the cover glass and lens to minimize the refractive index difference in the optical pathway. **b**, Demonstration of immersed-tip enhanced Raman measurement, enabling real-time measurements in liquid electrolytes. CCD, charge-coupled device. **c**, Alternative configurations for TERS that would allow operando measurement on opaque catalysts: (i) side excitation and collection and (ii) top excitation and collection. **d**, Simulated electric field distribution showing confined plasmonic fields in spectrally matched STM-TERS, leading to fine spatial resolution. **e**, Time-resolved Raman spectra monitored on a SnO_x surface during CO_2RR at different applied cathodic voltage (as marked). Persistence of the SnO_x A_{1g} band (for over 1 h) was observed up to -1.1 V. Credit: Figure adapted from ref. [32], American Chemical Society (**a**); ref. [44], Wiley (**b**); ref. [42], American Chemical Society (**c**); ref. [43], SNL (**d**); and ref. [20], American Chemical Society (**e**).

Raman cell usually features a viewing window above the catalyst surface. Compromise of excitation beam energy and flux must be made to optimize intensity while avoiding specimen damage. This viewing window is shared with incoming illumination in a confocal configuration. To achieve the best detection sensitivity, without distorting the electrochemistry, two different configurations are adopted. The first utilizes a high-numerical-aperture long-working-distance water-immersion objective[32]. The long-working-distance lens allows sufficient electrolyte and cover glass to be placed over the catalyst to avoid contamination. A water droplet is introduced between the lens and the cover glass to eliminate the air refractive index (n_{air}, Fig. 4a). The second solution utilizes a high-numerical-aperture short-working-distance lens wrapped and protected by an optically transparent thin Teflon film (n_{teflon} = 1.33, similar to water), allowing the lens to be immersed in electrolyte near the catalyst surface[33].

Thus far, the application of operando SERS in CO_2RR is confined to two categories: (a) monitoring the catalyst state and (b) identification of intermediate species. The high-speed data acquisition accessible to Raman spectroscopy helps in identifying metastable catalyst states and intermediates[30]. For example, operando Raman spectroscopy identifies SnO_2, not Sn(0), as the active surface for CO_2RR to formate (Fig. 4e)[20]. At –1.1 V, the A_{1g} mode of SnO_2 crystallites persist over 1 h, whilst formate is produced with a Faradaic efficiency greater than 80%. Operando SERS is also used to determine the catalyst state on oxide-derived Cu, Zn and mixed Cu–Zn catalysts[34,35]. It appears that the surfaces of these catalysts are reduced, within minutes, at CO_2RR-relevant potentials.

*CO is the most commonly observed CO_2RR intermediate using SERS on Cu and Ag surfaces[36–38], although less-intense carbonate and formate signals have also been observed[36–39]. Operando SERS is used to attribute the enhanced CO_2RR to CO on Ag surfaces to the weakening of the Ag–CO bond when 3,5-diamino-1,2,4-triazole (DAT) is added[40]. Isotope labelling can be used to confirm the peak assignment in Raman spectroscopy, as the harmonic oscillator model can predict the shift in the mode's frequency. For example, deuterium isotope labelling helped in confirming the C–H stretching vibration of the adsorbed formate (*HCOO) intermediate during operando Raman spectroscopy on Cu (ref. [41]).

The development of tip-enhanced Raman spectroscopy (TERS)[42] significantly improved intensity and spatial resolution of Raman, while allowing the probing of adsorbates at nanometre resolution. When coupled with a scanning tunnelling microscopy (STM) tip, the plasmon resonance can be tuned to match the downward transitions of the Raman scattering (Fig. 4d)[43], resulting in an intense enhancement factor at smaller incident photon flux. A tip and confocal arrangement is available for economical adaptation of an existing Raman setup (Fig. 4c). Most relevant to CO_2RR is probably the demonstration of TERS on an atomic force microscopy (AFM)-based tip in liquid through bottom illumination (Fig. 4b)[44]. An alternative strategy of stabilization and cryogenic trapping of intermediate phase approach was suggested[45], where Fe–CO_2 and Fe–CO_2H intermediates were isolated and probed at cryogenic temperature during the CO_2RR to CO on Fe(0)-porphyrin.

Overall, operando optical spectroscopy has largely succeeded in identifying intermediate species containing C–O, and has contributed significantly in refining reaction pathway selection for DFT calculations. Although simple and highly accessible, it has limited spatial resolution and is less sensitive to changes on the catalyst surface, therefore other techniques are required to complement it.

X-ray characterization techniques

Optical-based techniques can be complemented by X-ray techniques to overcome their limitations in probing catalyst surfaces.

With recent advances in current third-generation synchrotron radiation sources, operando hard and soft X-rays become increasingly applicable to catalysis, offering element-, orientation- and state-sensitive probing capabilities. Although direct demonstrations of operando X-ray techniques for CO_2RR are still limited, possibly due to setup complication or limited access to central facilities, they hold huge potential to solve issues (1) and (3) in the catalyst discovery process.

X-ray absorption spectroscopy. Probably one of the most widely used X-ray techniques for catalytic studies, X-ray absorption spectroscopy (XAS) allows for the examination of gas, liquid and solid samples. XAS spectrum collection is a relatively straightforward process, where the X-ray intensities are compared before and after interacting with specimens. Although XAS is generally insensitive towards lighter elements (for example, carbon), adsorbing species can be indirectly detected through monitoring minute changes in the catalyst state and coordination.

X-ray absorption near edge structure (XANES) focuses on the features within ±1% of the absorption edge, providing characteristic information on electron transition from occupied to unoccupied states. Pre-edge peak(s) can be present due to orbital hybridization induced by coordinating species (for example, ligands). The edge position is a primary indicator of the element's oxidation state because of its correlation to the effective nuclear charge. The oscillating intensity in the extended X-ray absorption fine structure (EXAFS) originates from interference effect between ejected and backscattered photoelectrons surrounding the absorbing atom, thus local structural information can be extracted[46]. Theoretical particle sizes can also be estimated from treated EXAFS data as the observed coordination number declines with decreasing size. Molecular dynamics simulation analyses of EXAFS data have demonstrated accurate determination of Pt nanoparticles in the range 17–70 Å (ref. [47]).

The larger penetration depth of hard X-rays required to match K-absorption edges allows flexible and real-time operando measurement of working electrocatalysts[48]. Figure 5a displays a typical operando X-ray electrochemical cell setup, where the catalyst is deposited onto an X-ray transparent support (for example, SiN_x) and signals can be measured in a fluorescence yield counter or through a spectrometer.

One key advantage of XAS is the ability to probe atom-specific structural information, even on extremely small and complex catalysts. For example, operando EXAFS has confirmed the atomic dispersion of single-atom Ni on N-doped graphene and shown its stability during CO_2RR (ref. [49]). Operando EXAFS measurement also reveals direct electronic modulation between the Co centre and the COF-367 covalent organic framework, allowing Co^{2+} to be partially reduced to Co^{+} (ref. [50]). Operando EXAFS is also sensitive to structural change, it can capture the complex restructuring of Cu(II)phthalocyanine to 2 nm Cu nanoclusters during CO_2RR (ref. [51]). Intriguingly, the nanoclusters revert back to Cu(II)phthalocyanine when the voltage is removed, suggesting reversibility for this process.

The hydrogen evolution reaction (HER) competes with CO_2RR in aqueous electrolyte, limiting the search for CO_2RR catalysts to those with minimal HER activity. However, the idea of producing syngas ($CO–H_2$ mixture) from CO_2RR expands the range of candidate materials, for example, Pd. In this case, background knowledge of Pd characterization using XAS (in conventional catalysis) helps the operando XAS interpretation of CO_2RR on Pd. The gradual peak shift to lower energy and white line intensity increase (sharp peak arising from the absorption edge) with increasing cathodic overpotential were immediately recognized as reversible H uptake, leading to β-PdH formation and longer Pd–Pd bond length[17]. What is interesting is that the presence of β-PdH during CO_2RR lowers the binding energy of both *CO and *H, and guard against CO poisoning. The result improved theoretical modelling and understanding of how Pd, perceived as a proficient HER catalyst, can be a CO_2RR promoter as well.

We note that the use of XAS is not limited to structural investigation. With the aid of computer post-processing, XAS signals can be used to construct 3D chemical tomography of working catalysts during electrochemical reactions. An operando computer tomography (CT)-XANES has been developed to investigate the degradation of a polymer electrolyte fuel cell. The root cause was pinpointed to migrating Pt catalyst into the proton exchange membrane, causing a short circuit (Fig. 5b)[52]. We envision that similar measurements can be extended to CO_2RR systems, providing insights on the catalysts' dynamic 3D spatial distribution and stability during catalysis.

X-ray photoelectron spectroscopy. When an electron gains enough energy from an incoming photon to be ejected to the continuum, a photoelectron is created and examinable by X-ray photoelectron spectroscopy (XPS). Both kinetic energy and the number of escaped electrons can be measured simultaneously from the sample surface of a few nanometres in depth, providing elemental composition, chemical and electronic state information of the catalyst. Due to the photoelectron's short inelastic mean free path (IMFP) in ambient conditions and to keep the analysed surface clean, XPS is typically performed in an ultra-high vacuum (UHV) environment, making the analysis of solid–liquid interface central to operando electrochemical study extremely difficult.

Basic analysis may be done by carefully transferring the catalyst under vacuum to an adjacent XPS chamber after electrocatalysis. Recently, this type of experiment was conducted on oxide-derived CO_2RR catalysts[53,54], revealing a possible presence of surface and subsurface oxygen after catalysis. However, the measurement could be affected by rapid interaction between the catalyst, electrolyte and oxygen during sample transfer in ambient conditions where electrochemistry is absent[55], limiting its usefulness.

An alternative strategy implementing a photoelectron-transparent graphene membrane as a pressure barrier has been proposed[56]. With a membrane-sealed cell, flow-cell electrochemistry may be performed while in UHV, paving the way for new techniques like operando photoemission electron microscopy (PEEM)[57].

Another reasonable approach is to separate the sample cell chamber and electron analyser via differential pumping and an electrostatic lens system[58]. This approach allows the sample chamber to be kept near atmospheric pressure and an unsealed electrochemical cell to be placed inside (Fig. 5c)[59]. The use of a synchrotron radiation source is recommended for ambient pressure X-ray photoelectron spectroscopy (APXPS) of the solid–liquid interface, as the incoming photon energy needs to be tuned to balance the photoelectron IMFP and photo-ionization cross-section. Even so, the electrolyte layer still needs to be thin enough (<20 nm) for meaningful measurement[60].

The dip-and-pull method (Fig. 5e) is a good strategy, where electrodes are pulled halfway through to the APXPS analysis chamber from the electrolyte reservoir[61]. The presence of a 10–30 nm electrolyte overlayer allows electrochemical bias to be applied during APXPS. However, the dip-and-pull strategy is not without weakness: it is difficult to get consistently thin electrolyte film, inevitably causing poor signal-to-noise ratio. Additionally, the thin layer of electrolyte is likely to induce concentration difference due to mass transport limitation[60]. The dip-and-pull strategy has been used to detect adventitious oxygen in reduced Cu catalysts[62]. Data fitting, assuming several flat overlayers of water, determined that most of the adventitious oxygen was Cu-bound. While the measurement was done completely inside APXPS chamber without air exposure, the proposed sub-surface oxygen interpretation should be taken with care, as rapid interaction between Cu and O in electrolyte was reported[55].

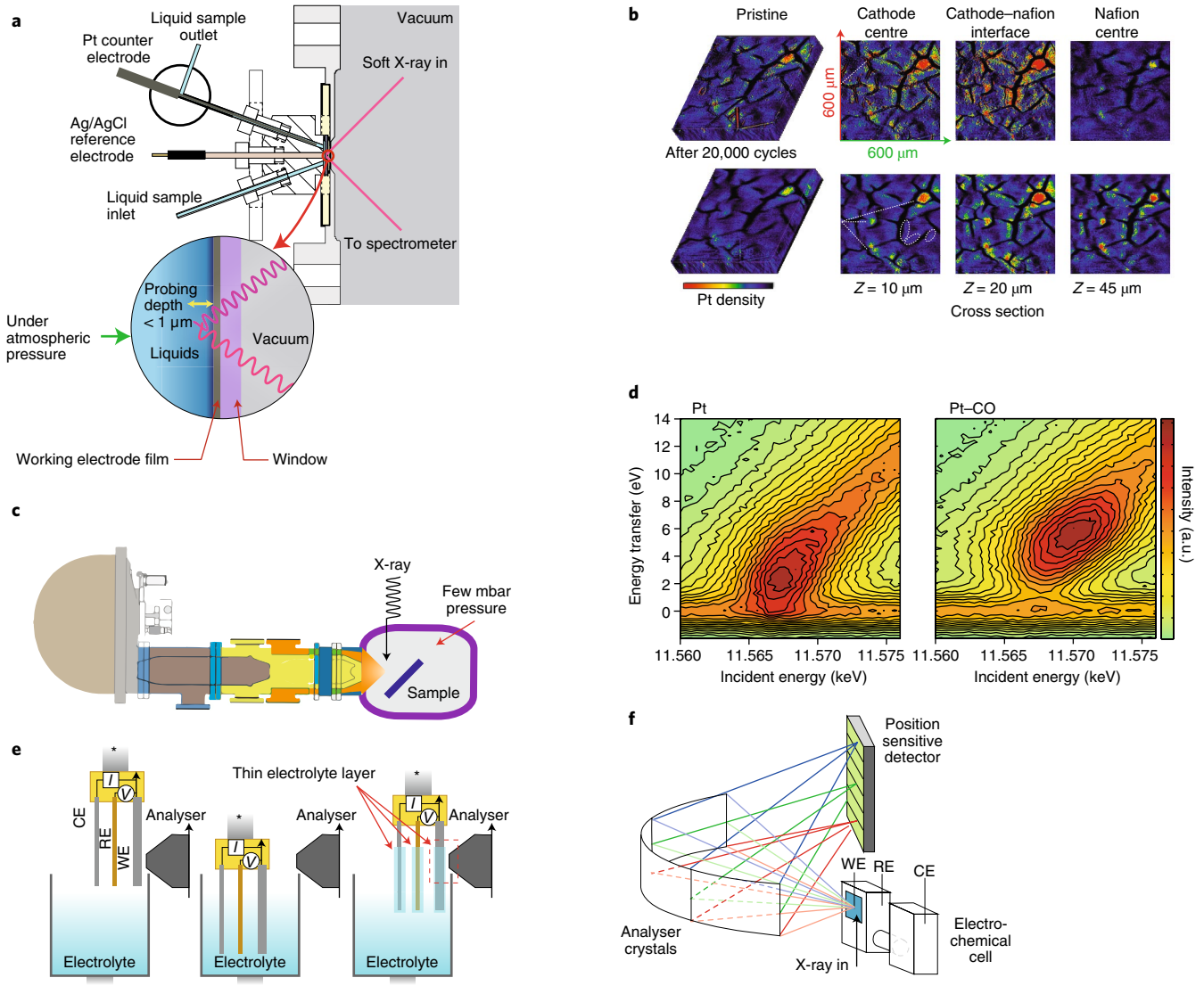

Fig. 5 | X-ray techniques for operando electrochemical measurements. a, Electrochemical flow cell configuration used for operando X-ray measurement. **b**, Operando XANES 3D tomography on polymer electrolyte fuel cell tracking Pt L_{III} edge intensity over a 600×600×90 μm³ fuel cell section before and after 20,000 cycles. Reconstruction of the 3D tomography at different depths reveals migration of dissolved Pt atoms into the Nafion membrane. Dotted lines and circles mark significant changes in Pt density. **c**, Differential pumping setup and membrane-covered cell setup for APXPS. **d**, In situ $2p_{3/2}$ RIXS planes of supported bare Pt nanoparticles and with CO adsorbed. **e**, An illustration of the dip-and-pull operando XPS strategy. **f**, Experimental setup for wavelength-dispersive IXS with an in situ electrochemical cell. WE, RE and CE denote working, reference and counter electrodes, respectively. Credit: Figure adapted from ref. [76], AIP Publishing (**a**); ref. [52], Wiley (**b**); ref. [59], Wiley (**c**); ref. [74], American Chemical Society (**d**); ref. [61], SNL (**e**); and ref. [78], RSC (**f**).

Oxide-derived catalyst case study. Obtained from electrochemical reduction of a higher oxidation state precursor, oxide-derived catalysts show significantly higher CO_2RR activity than the bare metallic variants[63,64]. The reason behind the enhanced performance has become the subject of contentious debate in recent years. We recognise that many operando CO_2RR studies are aimed at detecting residual oxygen or oxidized metal centres in oxide-derived catalysts, as the revelation of rapid interaction between electrolyte and catalyst[55] renders non-operando approaches less meaningful.

We previously discussed the detection of SnO_x at CO_2RR potential using operando Raman spectroscopy[20]. However, such detection may be restricted to highly conductive oxides that allow efficient electron transfer while remaining in oxidized form. On non-conductive oxide-derived catalysts, like CuO_x-derived Cu, residual surface oxides were not observed[35].

Using operando EXAFS, persistent Cu^+ signal has been detected on oxide-derived Cu under CO_2RR conditions[46,65]. Higher oxidation states of Fe and Co have been found stable using operando EXAFS during CO_2RR on greigite (Fe_3S_4; ref. [66]) and COF-367–Co framework[50], respectively. Additionally, the presence of adventitious oxygen, proposed to be Cu-bound, was also detected using operando APXPS (ref. [62]). These observations brought forth the idea that residual oxides can persist in the sub-surface instead. Several DFT calculation studies ensued; describing ways that residual oxygen could enhance the CO_2 chemisorption and thus CO_2RR (refs [67–69]).

However, the premise to the residual oxide benefit to CO_2RR is its stability under cathodic conditions. Most recent DFT studies indicate that sub-surface oxygen is unlikely to survive under CO_2RR conditions[70,71], although it has been suggested that it can be stabilized on a reduced Cu-nanocube model[72].

The complex issue of oxide-derived catalysts highlights the challenges faced in interpreting operando measurements, as assumptions drawn from a very controlled environment may not reflect the complex CO_2RR condition. To resolve this issue, we believe that new operando approaches beyond the conventional IR, Raman, XPS and XAS are required to provide experimental evidence on sub-surface oxygen that is capable of influencing intermediate binding[71].

Emerging opportunities from contemporary X-ray techniques. We have elaborated the importance of operando X-ray techniques in addressing basic questions in CO_2RR. However, conventional XAS techniques suffer from intrinsic broadening of the core–hole lifetime, which can be as much as 5–10 eV for metal L-edges[73]. Spectra overlap from multiple scatterers often leads to poor atomic and energy resolution, as XAS only gives averaged structural information.

In this regard, it is desirable to use a high-resolution monochromator to discriminate finer energy resolution in inelastic X-ray scattering (IXS). An excellent example of this technique's strength is the in situ observation of changing Pt valence *d*-band originating from newly formed bonding and antibonding orbitals as CO is adsorbed onto Pt (Fig. 5d)[74]. Such a feat is only achievable by consecutive measurements of X-ray emission at different energies while the excitation X-ray is at resonance with the Pt L_3 edge. This subset is termed resonant inelastic X-ray scattering (RIXS). RIXS measurement, especially near the metal L-edge, allows element-selective probing of *d*–*d* excitations and reliable determination of the metal–ligand field and chemical processes[75]. This technique has strong potential to address issues (1), (2) and (3), especially when coupled with careful theoretical analysis to de-convolute polarization and momentum transfer information.

The low intensity of RIXS signal has mostly been overcome by the recent development of third-generation synchrotron facilities and advanced cell construction that allows low-energy photon-out measurements[76,77]. Recently, a new wavelength dispersive setup consisting of analyser crystal and position sensitive detector setup has been used to perform operando K-edge IXS on mixed $MnNiO_x$ oxygen evolution reaction (OER) catalyst (Fig. 5f)[78]. The experiment was able to determine that the MnO_x and NiO_x do not share the same atomic environment, and the presence of Ni appears to stabilize MnO_x by inducing earlier oxidation on the latter. We foresee that (R)IXS experiments could help to determine the presence of residual oxide in CO_2RR, as compatible setups have been developed[65].

Another relevant technique for CO_2RR is surface X-ray scattering (SXS), which can provide information about the abrupt termination of crystalline surfaces as well as adsorbed groups. For example, the oxidation and reduction behaviour of Pt(111) surfaces under electrochemical conditions have been investigated in situ using SXS (ref. [79]). Pt(111) experienced surface buckling at the top layer due to oxygen and hydroxyl adsorption at 0.95 V versus reversible hydrogen electrode (RHE), causing attenuation in the scattered intensities.

Diffraction anomalous fine structure (DAFS) is a relatively recent technique that combines crystallographic X-ray diffraction with spectroscopic XAS. When combined, DAFS can provide XAS with a set of atoms in a specific site/phase on the catalyst (as controlled by the diffraction signal). Bouldin et al. described this technique more elegantly as an "(E)XAFS with virtual photoelectrons"[80]. The typical beamline setup involves a second X-ray detector that can rotate around the sample, providing 2θ resolution. DAFS is extremely useful in distinguishing contributions for the same type of atom existing in inequivalent sites within the unit cell, as well as in different phase, or detect changes in the cell lattice. An excellent example would be the identification of the Ni atom aggregates within a $Li_{1-x}Ni_{1+x}O_2$ interlayer during lithium battery electrode charge–discharge cycling, which cannot be distinguished from NiO_2 host otherwise[81]. Although DAFS has only been demonstrated on bulk samples, grazing incidence measurement can enable surface measurements. We believe that DAFS has the potential to shed light into the short–medium range environment of a specific atom on a particular catalyst phase (for example, in the case of alloys[82]) or different orientation.

Electron-based characterization techniques

Electron-based techniques encompass electron microscopy and detection of electronic signals by static or scanning probes. These are important characterization tools that can track minute changes in catalyst (down to unit cell level), localized electrochemical activity and electron transfer processes at the catalyst surface, potentially elucidating issues (1), (3) and (4).

Liquid phase–transmission electron microscopy. In situ liquid phase–transmission electron microscopy (LP–TEM) techniques are very useful in tracking real-time physical migration, morphological evolution and, sometimes, compositional change under modulated environment in synthetic or catalytic processes. Modern LP–TEM holders allow the introduction of larger amounts of flowing electrolyte around the main observation microcell while maintaining compatibility with the UHV chamber (Fig. 6a,b). The back electrolyte contact effectively provides a larger counter electrode to enable higher current density to be applied on the working electrode. This setup provides some respite for examining diffusion-limited reactions like CO_2RR. SiN_x is the current prime choice for TEM windows due to its electron transparency and high flexural strength.

In our view, in situ electrochemical-TEM measurements are very much a work-in-progress, as the compromise needed to match actual electrocatalysis conditions is too great for this technique to be considered a fully operando measurement. For example, the limited space and positioning of the electrodes inside can cause non-uniform electric field distribution and create hot spots that artificially enhance electrochemical activity near the electrode tip[83]. Further, the electron beam is known to induce radiolysis and specimen damage[84]. However, we see value in this technique, as in situ LP–TEM can record atomic and morphological changes under electrochemical condition almost instantly, at high resolution. This would provide valuable information on how the catalyst surface is transformed or degraded during catalytic reaction, useful to address issue (1).

Most in situ LP–TEM experiments are demonstrated on non-CO_2RR systems, taking advantage of electron-beam induced transformation such as nanoparticle nucleation, growth, dissolution, coalescence and so on[84]. For example, numerous studies assess the stability of OER catalysts upon contact with water and electron beam[85]. Often these studies report nucleation of oxygenated species inside the in situ LP–TEM cell that would not be possible without the presence of oxygen (radical) species believed to be OER intermediates (Fig. 6c,d)[86]. Another useful approach is the one-to-one correspondence approach, where the trajectory, morphology and chemical state of catalysts can be probed in 3D using electron tomography after aging outside the UHV chamber[87]. In situ LP–TEM is also suitable to observe catalyst degradation by dissolution and mechanical dislodgement (Fig. 6e,f)[84].

In situ TEM can also be utilized to study the surface oxidation behaviour of a catalyst. For example, the surface oxidation of Pd nanocrystals was found to initiate at the atomic steps or vertex site, then proceed preferentially on the $(111)_{Pd}$ faces (Fig. 6g)[88]. These surfaces also show significantly higher reactivity[89], thus in situ TEM may be used to look for catalytically active surfaces.

Though there is no direct example of studying CO_2RR using operando TEM so far, we see significant advantages in doing so. A good example would be the use of electron tomography to get a better estimate of active surface area/possible active sites, and to study core–shell structures of bimetallic origin, with the possibility of obtaining 3D, instead of the usual 2D, visualization[90].

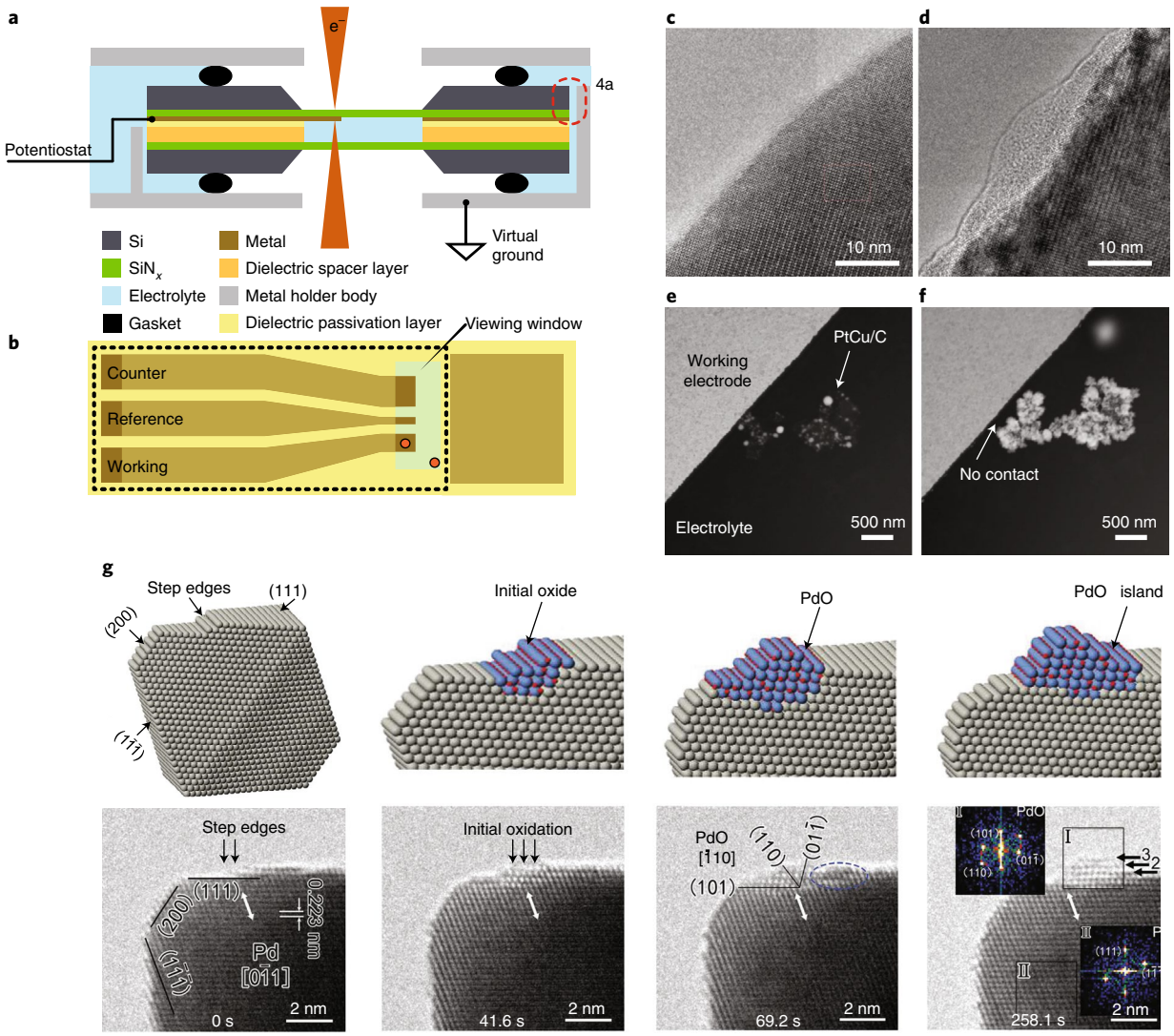

Fig. 6 | Progress of in situ liquid phase TEM measurements. a,**b**, An illustration of recent in situ LP–TEM electrochemical cell design in cross-sectional (**a**) and plan (**b**) view, with an enlarged electrolyte reservoir to improve the anode contact area (dotted lines) while maintaining a thin viewing window area. **c**,**d**, Pristine $Pr_{0.64}Ca_{0.36}MnO_3$ (PCMO) in vacuum (**c**) and after 120 s exposure to 0.3 mbar H_2O/He/SiH_4 mixture at an electron flux of 11,000 e Å^{-2} s^{-1} (**d**). The nucleation of amorphous SiO_{2-x} overgrowth in **d** indicates oxygen evolution reaction on PCMO surface under electron beam stimuli. **e**, Observation of dislodged PtCu/C catalyst in in situ LP–TEM. **f**, Pt was subsequently deposited on the surface due to electron beam bias. **g**, Molecular structure model and time-resolved in situ TEM showing Pd catalyst oxidation at 6.8×10^{-5} Pa O_2. Credit: Figure adapted from ref. [118], ECS (**a**,**b**); ref. [86], American Chemical Society (**c**,**d**); ref. [84], American Chemical Society (**e**,**f**); and ref. [88], RSC (**g**).

Scanning probe microscopy. Scanning probe microscopy (SPM) techniques were originally devised to probe surface information of samples using a fine-tipped probe. Their initial form, scanning tunnelling microscopy (STM), allows imaging of a surface at the atomic level from detection of quantum tunnelling current[91]. Modification to the STM design allows the measurement of tunnelling electrons in electrochemical condition[92], potentially allowing the detection of surface atom variation under catalytic condition and suitable to address issues (1) and (3). In fact, operando EC–STM measurements have detected Cu surface atomic reconstructions in electrochemical condition[93].

AFM enables surface profiling by detection of the atomic force interaction between the tip and the sample[94]. The imaging resolution is poorer compared to STM, but the tip can now serve an additional function as electrochemical potential or current sensor while imaging. An excellent demonstration of this technique is the operando observation of microscopic surface reconstructions during CO_2RR catalysis (Fig. 7f)[95] and operando identification of cobalt (oxy)hydroxide phosphate's dual function as hole collector and water oxidation catalyst in photoelectrocatalytic system[96].

Scanning electrochemical microscopy (SECM) is a different variation of the SPM technique, where the scanning tip acts as a miniaturized electrode to conduct investigation of local electrochemical behaviour of liquid/solid/gas interfaces, suitable to address issues (2) and (5), but without topographic imaging capabilities[97]. Seminal work was performed by Bard and co-workers using SECM to differentiate flat glass and Pt surfaces[98]. When combined with nonlinear a.c. electrochemical measurements such as electrochemical impedance spectroscopy (EIS), it is possible to probe local environments of the catalyst surface immediately under the microelectrode, addressing issue (5) (Fig. 7e). In particular, the electrochemical and charge transfer behaviour of different exposing facets, an indication of their reactivity, can also be revealed[99,100]. More recently, SECM was used to probe the enhanced CO_2RR activity on Au surfaces

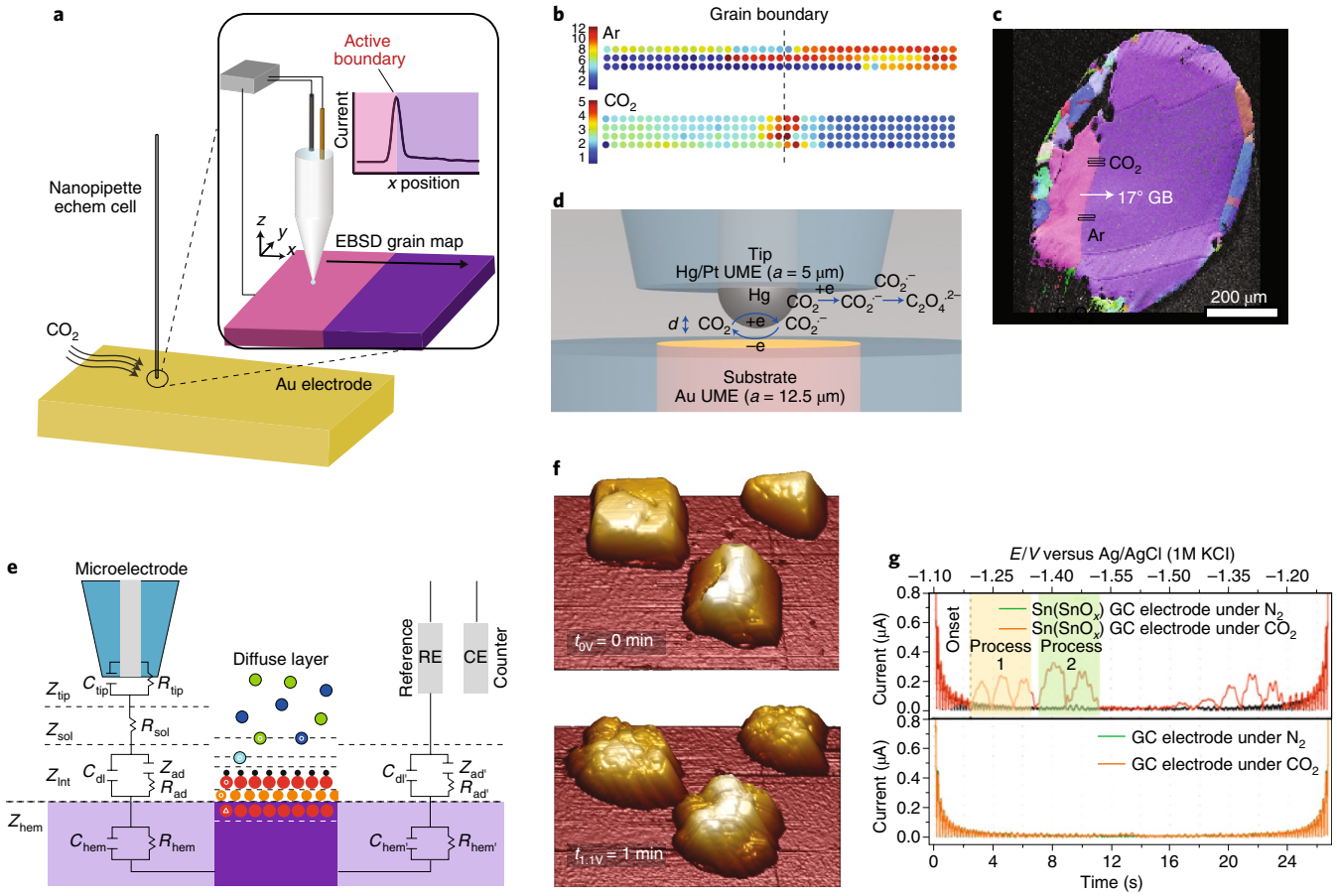

Fig. 7 | Scanning-probe-microscopy-based techniques for operando electrochemical measurements. a–c, The use of SECM in detecting CO_2RR activity on an Au electrode grain boundary (**a**), with a corresponding electrocatalytic current heat map (**b**) near the grain boundary (dashed lines added) as marked on the electron backscattered micrograph (**c**). **d**, Schematics of Hg/Pt ultra-micro electrode (UME) and Au UME substrate setup to generate and detect the $*CO_2^-$ intermediate and its dimer. **e**, Schematics of SECM detecting local electrochemical impedance. **f**, Operando EC-AFM micrograph showing significant morphological change of $CuCl_x$-Cu_2O during CO_2RR. **g**, Fifth harmonic components of FTAC voltammograms, displayed in both time (lower *x* axis) and potential (upper *x* axis) formats, highlighting two distinct electron transfer process occurring just after the onset potential around -1.18 V versus Ag/AgCl on a $Sn(SnO_x)$-modified glassy carbon (GC) electrode. Baseline measurement on an unmodified GC electrode under CO_2 or N_2 purging (bottom voltammogram) shows no such process. Credit: Figure adapted from ref. [101], AAAS (**a–c**); ref. [102], American Chemical Society (**d**); ref. [99], American Chemical Society (**e**); ref. [95], Wiley (**f**); and ref. [106], American Chemical Society (**g**).

receiving different treatments[101]. Combined with Rutherford backscattering (RBS) electron micrograph imaging, clear indication of increased CO_2RR activity was found to occur near the grain boundary (Fig. 7a–c).

Using a Hg/Pt ultramicroelectrode (UME) probe, it was possible to detect the $*CO_2^-$ intermediate and its dimerization on the Au UME substrate[102]. $*CO_2^-$ is constantly being generated at the Hg/Pt probe and, owing to the low binding energy, this intermediate is transferred to the Au UME substrate (located 0.2–5 μm away) to be analysed (Fig. 7d). The dimerization rate was assessed to be 6.0×10^8 M^{-1} s^{-1} with a half-life of 10 ns by fitting the experimental data with a theoretical simulation, opening up the possibility of using SECM to study the CO_2RR mechanism.

Electrochemical techniques in catalysis are usually limited to d.c., where a constant or variable field is applied on the surface of catalysts. However, Fourier transform a.c. spectroscopy (FTAC) is a powerful electrochemical technique that can interrogate fast Faradaic processes within the double layer region, thus confronting issue (4)[103]. FTAC has high kinetic sensitivity — the current magnitude of the nonlinear higher harmonic components increases significantly with faster electron transfer kinetics[104]. Under d.c.-only voltammetry conditions, the low-level Faradaic process would have been shrouded by other slower process (for example, redox) or double layer charge–discharge behaviour.

FTAC has been used to confirm fast and reversible charge transfer in $[\alpha\text{-}SiW_{12}O_{40}]^{6+/7+}$, confirming its role as redox mediator in the reduction of CO_2 to CO on Ag nanoclusters capped with bovine serum albumin in DMF (ref. [105]). More recently, this technique has shed some light into the electron transfer during CO_2RR. A sharp (two-step, shown as a doublet and triplet) fifth harmonic of the FTAC indicates that the CO_2RR onset (–1.2 V versus Ag/AgCl; Fig. 7g) involves a two-electron transfer process. This could point to the reduction of either $*CO_2$ or $*H_2CO_3$ intermediates during CO_2 conversion to formate on SnO_x surfaces[106]. We propose that, when combined with SECM-based microelectrodes, FTAC is a powerful technique that can discern fast processes in different facets or less-defined active areas (for example, roughened Cu).

Prospects and outlook

Operando measurements have contributed tremendously to our understanding of CO_2RR. Most recently, new waves of theoretical studies aimed at fully decoupling the electric field and ionic effects

have been inspired by findings from operando measurements[24,107]. However, more can be done to further the capabilities of currently available techniques. Recently discovered graphene-enhanced Raman spectroscopy (GERS) offers the promise of molecular-selective Raman enhancement[108]. This may prove interesting for CO_2RR as intermediates may be transferred from the active sites onto graphene for subsequent GERS measurement.

Another intriguing possibility is the use of in situ LP–TEM with more-precise control over the radiolysis process. Recently, it has been proposed that the problematic radiolytic process can instead be a way to generate relevant reaction intermediates during in situ LP–TEM measurements[109]. This means that, the electron beam can be viewed as a very fine ionizing radiation source that provides rational chemical perturbation of a material system. The radiolytic species and radicals generated in water are similar to the water splitting intermediates (H•, H_2, H_2O_2, OH• and O_2), and altering the electron dose can control their concentration[110]. With more understanding of radiolytic generation on various solvents and intermediates, we envision that in situ LP–TEM will be of particular interest in understanding CO_2RR where the photolytic generation of intermediates can be reproduced using an electron beam.

We also predict the rising importance of RIXS as the field of CO_2RR moves beyond single transition metal catalysts, to explore non-metal catalysts like doped carbon[111] or multi-metallic hybrid structures like Cu_3Y–Ni, Cu_3Sc–Ni (ref. [112]) or Ni–Ga alloys[113]. High resolution RIXS is probably the only technique capable of providing direct experimental proof on the preferred adsorption geometry of adsorbates[114].

We believe data collected through operando techniques can be added into bulk structure databases to feed into machine-learning-aided prediction of adsorption energy, which can reduce the number of single point DFT calculations required to identify viable candidates[113,115]. Future investigation of these new catalyst materials using advanced operando techniques is crucial in addressing the scientific challenge and closing the catalytic discovery loop. Overall, we hope that these concerted efforts will bring us closer towards creating a closed-loop anthropogenic carbon cycle and a more secure energy future for humanity.

Received: 20 May 2018; Accepted: 18 October 2018;
Published online: 10 December 2018

References

1. *UNFCCC Report of the Conference of the Parties on its Twenty-First Session, Held in Paris from 30 November to 13 December 2015* Decision 1/CP.21 (United Nations, 2015).
2. van Vuuren, D. P. et al. Alternative pathways to the 1.5 °C target reduce the need for negative emission technologies. *Nat. Clim. Change* **8**, 391–397 (2018).
3. Graves, C., Ebbesen, S. D., Mogensen, M. & Lackner, K. S. Sustainable hydrocarbon fuels by recycling CO_2 and H_2O with renewable or nuclear energy. *Renew. Sustain. Energy Rev.* **15**, 1–23 (2011).
4. Seh, Z. W. et al. Combining theory and experiment in electrocatalysis: Insights into materials design. *Science* **355**, eaad4998 (2017).
5. Kuhl, K. P., Cave, E. R., Abram, D. N. & Jaramillo, T. F. New insights into the electrochemical reduction of carbon dioxide on metallic copper surfaces. *Energy Environ. Sci.* **5**, 7050–7059 (2012).
6. Kortlever, R., Shen, J., Schouten, K. J. P., Calle-Vallejo, F. & Koper, M. T. M. Catalysts and reaction pathways for the electrochemical reduction of carbon dioxide. *J. Phys. Chem. Lett.* **6**, 4073–4082 (2015).
7. Goldsmith, B. R., Esterhuizen, J., Liu, J.-X., Bartel, C. J. & Sutton, C. Machine learning for heterogeneous catalyst design and discovery. *AlChE J.* **64**, 2311–2323 (2018).
8. Hansen, H. A., Varley, J. B., Peterson, A. A. & Nørskov, J. K. Understanding trends in the electrocatalytic activity of metals and enzymes for CO_2 reduction to CO. *J. Phys. Chem. Lett.* **4**, 388–392 (2013).
9. Peterson, A. A., Abild-Pedersen, F., Studt, F., Rossmeisl, J. & Norskov, J. K. How copper catalyzes the electroreduction of carbon dioxide into hydrocarbon fuels. *Energy Environ. Sci.* **3**, 1311–1315 (2010).
10. Kirk, C. et al. Theoretical investigations of the electrochemical reduction of CO on single metal atoms embedded in graphene. *ACS Cent. Sci.* **3**, 1286–1293 (2017).
11. Wain, A. J. & O'Connell, M. A. Advances in surface-enhanced vibrational spectroscopy at electrochemical interfaces. *Adv. Phy. X* **2**, 188–209 (2017).
12. Yang, C. & Wöll, C. IR spectroscopy applied to metal oxide surfaces: adsorbate vibrations and beyond. *Adv. Phy. X* **2**, 373–408 (2017).
13. Wuttig, A., Yaguchi, M., Motobayashi, K., Osawa, M. & Surendranath, Y. Inhibited proton transfer enhances Au-catalyzed CO_2-to-fuels selectivity. *Proc. Natl Acad. Sci. USA* **113**, E4585–E4593 (2016).
14. Hori, Y., Koga, O., Yamazaki, H. & Matsuo, T. Infrared spectroscopy of adsorbed CO and intermediate species in electrochemical reduction of CO_2 to hydrocarbons on a Cu electrode. *Electrochim. Acta* **40**, 2617–2622 (1995).
15. Gunathunge, C. M., Ovalle, V. J., Li, Y., Janik, M. J. & Waegele, M. M. Existence of an electrochemically inert CO population on Cu electrodes in alkaline pH. *ACS Catal.* **8**, 7507–7516 (2018).
Observation of two different $*CO_{ads}$ geometries, and demonstration that $*CO_{bridge}$ is inactive for further reduction using operando IR spectroscopy. Relates to the deactivation and surface reconstruction of Cu during electrocatalysis.
16. Dunwell, M., Yan, Y. & Xu, B. In situ infrared spectroscopic investigations of pyridine-mediated CO_2 reduction on Pt electrocatalysts. *ACS Catal.* **7**, 5410–5419 (2017).
17. Sheng, W. et al. Electrochemical reduction of CO_2 to synthesis gas with controlled CO/H_2 ratios. *Energy Environ. Sci.* **10**, 1180–1185 (2017).
18. Firet, N. J. & Smith, W. A. Probing the reaction mechanism of CO_2 electroreduction over Ag films via operando infrared spectroscopy. *ACS Catal.* **7**, 606–612 (2017).
19. Baruch, M. F., Pander, J. E., White, J. L. & Bocarsly, A. B. Mechanistic insights into the reduction of CO_2 on tin electrodes using in situ ATR-IR spectroscopy. *ACS Catal.* **5**, 3148–3156 (2015).
20. Dutta, A., Kuzume, A., Rahaman, M., Vesztergom, S. & Broekmann, P. Monitoring the chemical state of catalysts for CO_2 electroreduction: an in operando study. *ACS Catal.* **5**, 7498–7502 (2015).
21. Murata, A. & Hori, Y. Product selectivity affected by cationic species in electrochemical reduction of CO_2 and CO at a Cu electrode. *Bull. Chem. Soc. Jpn* **64**, 123–127 (1991).
22. Dunwell, M. et al. The central role of bicarbonate in the electrochemical reduction of carbon dioxide on gold. *J. Am. Chem. Soc.* **139**, 3774–3783 (2017).
Demonstrates that bicarbonate is the primary source of carbon in the CO formed at the Au electrode through equilibrium exchange with dissolved CO_2 using operando ATR-SEIRAS.
23. Zhu, S., Jiang, B., Cai, W.-B. & Shao, M. Direct observation on reaction intermediates and the role of bicarbonate anions in CO_2 electrochemical reduction reaction on Cu surfaces. *J. Am. Chem. Soc.* **139**, 15664–15667 (2017).
24. Resasco, J. et al. Promoter effects of alkali metal cations on the electrochemical reduction of carbon dioxide. *J. Am. Chem. Soc.* **139**, 11277–11287 (2017).
25. Resasco, J., Lum, Y., Clark, E., Zeledon, J. Z. & Bell, A. T. Effects of anion identity and concentration on electrochemical reduction of CO_2. *ChemElectroChem* **5**, 1064–1072 (2018).
26. Pérez-Gallent, E., Marcandalli, G., Figueiredo, M. C., Calle-Vallejo, F. & Koper, M. T. M. Structure- and potential-dependent cation effects on CO reduction at copper single-crystal electrodes. *J. Am. Chem. Soc.* **139**, 16412–16419 (2017).
27. Lum, Y., Cheng, T., Goddard, W. A. & Ager, J. W. Electrochemical CO reduction builds solvent water into oxygenate products. *J. Am. Chem. Soc.* **140**, 9337–9340 (2018).
Demonstration of the involvement of O atoms from water in producing oxygenate products from CO_2. This calls into question previous models of oxygenate formation as O atoms in oxygenates have always been presumed to originate from CO_2 (or CO) intermediate.
28. Pérez-Gallent, E., Figueiredo, M. C., Calle-Vallejo, F. & Koper, M. T. M. Spectroscopic observation of a hydrogenated CO dimer intermediate during CO reduction on Cu(100) electrodes. *Angew. Chem. Int. Ed.* **129**, 3675–3678 (2017).
The initial observation of hydrogenated CO dimer (*OCCOH) on $(100)_{cu}$ using operando IR spectroscopy.
29. Schouten, K. J. P., Qin, Z., Gallent, E. P. & Koper, M. T. M. Two pathways for the formation of ethylene in CO reduction on single-crystal copper electrodes. *J. Am. Chem. Soc.* **134**, 9864–9867 (2012).
30. Deng, Y. & Yeo, B. S. Characterization of electrocatalytic water splitting and CO_2 reduction reactions using in situ/operando raman spectroscopy. *ACS Catal.* **7**, 7873–7889 (2017).
31. Albrecht, M. G. & Creighton, J. A. Anomalously intense Raman spectra of pyridine at a silver electrode. *J. Am. Chem. Soc.* **99**, 5215–5217 (1977).

32. Zeng, Z.-C. et al. Novel electrochemical Raman spectroscopy enabled by water immersion objective. *Anal. Chem.* **88**, 9381–9385 (2016).
33. Yeo, B. S., Klaus, S. L., Ross, P. N., Mathies, R. A. & Bell, A. T. Identification of hydroperoxy species as reaction intermediates in the electrochemical evolution of oxygen on gold. *ChemPhysChem* **11**, 1854–1857 (2010).
34. Ren, D., Ang, B. S.-H. & Yeo, B. S. Tuning the selectivity of carbon dioxide electroreduction toward ethanol on oxide-derived Cu_xZn catalysts. *ACS Catal.* **6**, 8239–8247 (2016).
35. Ren, D. et al. Selective electrochemical reduction of carbon dioxide to ethylene and ethanol on copper(I) oxide catalysts. *ACS Catal.* **5**, 2814–2821 (2015).
36. Oda, I., Ogasawara, H. & Ito, M. Carbon monoxide adsorption on copper and silver electrodes during carbon dioxide electroreduction studied by infrared reflection absorption spectroscopy and surface-enhanced Raman spectroscopy. *Langmuir* **12**, 1094–1097 (1996).
37. Ichinohe, Y., Wadayama, T. & Hatta, A. Electrochemical reduction of CO_2 on silver as probed by surface-enhanced Raman scattering. *J. Raman Spectrosc.* **26**, 335–340 (1995).
38. Mahoney, M. R., Howard, M. W. & Cooney, R. P. Carbon dioxide conversion to hydrocarbons at silver electrode surfaces: Raman spectroscpic evidence for surface carbon intermediates. *Chem. Phys. Lett.* **71**, 59–63 (1980).
39. Smith, B. D., Irish, D. E., Kedzierzawski, P. & Augustynski, J. A surface enhanced Raman scattering study of the intermediate and poisoning species formed during the electrochemical reduction of CO_2 on Copper. *J. Electrochem. Soc.* **144**, 4288–4296 (1997).
40. Schmitt, K. G. & Gewirth, A. A. In situ surface-enhanced Raman spectroscopy of the electrochemical reduction of carbon dioxide on silver with 3,5-diamino-1,2,4-triazole. *J. Phys. Chem. C* **118**, 17567–17576 (2014).
41. Deng, Y. et al. On the role of sulfur for the selective electrochemical reduction of CO_2 to formate on CuS_x catalysts. *ACS Appl. Mater. Interfaces* **10**, 28572–28581 (2018).
42. Zhang, Z., Sheng, S., Wang, R. & Sun, M. Tip-enhanced Raman spectroscopy. *Anal. Chem.* **88**, 9328–9346 (2016).
43. Zhang, R. et al. Chemical mapping of a single molecule by plasmon-enhanced Raman scattering. *Nature* **498**, 82–86 (2013).
44. Schmid, T., Yeo, B. S., Leong, G., Stadler, J. & Zenobi, R. Performing tip-enhanced Raman spectroscopy in liquids. *J. Raman Spectrosc.* **40**, 1392–1399 (2009).
45. Mondal, B., Rana, A., Sen, P. & Dey, A. Intermediates Involved in the $2e^-/2H^+$ Reduction of CO_2 to CO by iron(0) porphyrin. *J. Am. Chem. Soc.* **137**, 11214–11217 (2015).
46. Mistry, H. et al. Highly selective plasma-activated copper catalysts for carbon dioxide reduction to ethylene. *Nat. Commun.* **7**, 12123 (2016).
47. Clausen, B. S. et al. A new procedure for particle size determination by EXAFS based on molecular dynamics simulations. *J. Catal.* **141**, 368–379 (1993).
48. Eilert, A., Roberts, F. S., Friebel, D. & Nilsson, A. Formation of copper catalysts for CO_2 reduction with high ethylene/methane product ratio investigated with in situ X-ray absorption spectroscopy. *J. Phys. Chem. Lett.* **7**, 1466–1470 (2016).
49. Jiang, K. et al. Isolated Ni single atoms in graphene nanosheets for high-performance CO_2 reduction. *Energy Environ. Sci.* **11**, 893–903 (2018).
50. Lin, S. et al. Covalent organic frameworks comprising cobalt porphyrins for catalytic CO_2 reduction in water. *Science* **349**, 1208–1213 (2015).
51. Weng, Z. et al. Active sites of copper-complex catalytic materials for electrochemical carbon dioxide reduction. *Nat. Commun.* **9**, 415 (2018).
52. Matsui, H. et al. Operando 3d visualization of migration and degradation of a platinum cathode catalyst in a polymer electrolyte fuel cell. *Angew. Chem. Int. Ed.* **56**, 9371–9375 (2017).
53. Mistry, H. et al. Enhanced carbon dioxide electroreduction to carbon monoxide over defect-rich plasma-activated silver catalysts. *Angew. Chem. Int. Ed.* **56**, 11394–11398 (2017).
54. Gao, D. et al. Plasma-activated copper nanocube catalysts for efficient carbon dioxide electroreduction to hydrocarbons and alcohols. *ACS Nano* **11**, 4825–4831 (2017).
55. Lum, Y. & Ager, J. W. Stability of residual oxides in oxide-derived copper catalysts for electrochemical CO_2 reduction investigated with ^{18}O labeling. *Angew. Chem. Int. Ed.* **57**, 551–554 (2018).
56. Velasco-Velez, J. J. et al. Photoelectron spectroscopy at the graphene–liquid interface reveals the electronic structure of an electrodeposited cobalt/graphene electrocatalyst. *Angew. Chem. Int. Ed.* **54**, 14554–14558 (2015).
57. Nemšák, S. et al. Interfacial electrochemistry in liquids probed with photoemission electron microscopy. *J. Am. Chem. Soc.* **139**, 18138–18141 (2017).
58. Siegbahn, H. & Siegbahn, K. ESCA applied to liquids. *J. Electron. Spectrosc. Relat. Phenom.* **2**, 319–325 (1973).
59. Roy, K., Artiglia, L. & Bokhoven, J. A. V. Ambient pressure photoelectron spectroscopy: opportunities in catalysis from solids to liquids and introducing time resolution. *ChemCatChem* **10**, 666–682 (2018).
60. Liu, Z. & Bluhm, H. in *Hard X-ray Photoelectron Spectroscopy (HAXPES)* (ed Joseph Woicik) 447–466 (Springer International Publishing, 2016).
61. Axnanda, S. et al. Using "tender" X-ray ambient pressure X-ray photoelectron spectroscopy as a direct probe of solid-liquid interface. *Sci. Rep.* **5**, 9788 (2015).
62. Eilert, A. et al. Subsurface oxygen in oxide-derived copper electrocatalysts for carbon dioxide reduction. *J. Phys. Chem. Lett.* **8**, 285–290 (2017).
63. Gao, S. et al. Partially oxidized atomic cobalt layers for carbon dioxide electroreduction to liquid fuel. *Nature* **529**, 68–71 (2016).
64. Li, C. W., Ciston, J. & Kanan, M. W. Electroreduction of carbon monoxide to liquid fuel on oxide-derived nanocrystalline copper. *Nature* **508**, 504–507 (2014).
65. De Luna, P. et al. Catalyst electro-redeposition controls morphology and oxidation state for selective carbon dioxide reduction. *Nat. Catal.* **1**, 103–110 (2018).
Experimental demonstration of higher Cu oxidation state using in situ soft XAS. Time-dependant spectra of Cu^+ at CO_2RR relevant potentials were tracked for up to one hour.
66. Zakaria, S. N. A. et al. Insight into nature of iron sulfide surfaces during the electrochemical hydrogen evolution and CO_2 reduction reactions. *ACS Appl. Mater. Interfaces* **10**, 32078–32085 (2018).
67. Favaro, M. et al. Subsurface oxide plays a critical role in CO_2 activation by Cu(111) surfaces to form chemisorbed CO_2, the first step in reduction of CO_2. *Proc. Natl Acad. Sci. USA* **114**, 6706–6711 (2017).
68. Xiao, H., Goddard, W. A., Cheng, T. & Liu, Y. Cu metal embedded in oxidized matrix catalyst to promote CO_2 activation and CO dimerization for electrochemical reduction of CO_2. *Proc. Natl Acad. Sci. USA* **114**, 6685–6688 (2017).
69. Zhang, Y.-J. & Peterson, A. A. Oxygen-induced changes to selectivity-determining steps in electrocatalytic CO_2 reduction. *Phys. Chem. Chem. Phys.* **17**, 4505–4515 (2015).
70. Garza, A. J., Bell, A. T. & Head-Gordon, M. Is subsurface oxygen necessary for the electrochemical reduction of CO_2 on copper? *J. Phys. Chem. Lett.* **9**, 601–606 (2018).
71. Fields, M., Hong, X., Nørskov, J. K. & Chan, K. Role of subsurface oxygen on Cu surfaces for CO_2 electrochemical reduction. *J. Phys. Chem. C* **122**, 16209–16215 (2018).
72. Liu, C. et al. Stability and effects of subsurface oxygen in oxide-derived Cu catalyst for CO_2 reduction. *J. Phys. Chem. C* **121**, 25010–25017 (2017).
73. Penner-Hahn, J. E. in *eLS* Ch. 2.13 (John Wiley and Sons, London, 2005).
74. Glatzel, P., Singh, J., Kvashnina, K. O. & van Bokhoven, J. A. In situ characterization of the 5d density of states of Pt nanoparticles upon adsorption of CO. *J. Am. Chem. Soc.* **132**, 2555–2557 (2010).
75. van Schooneveld, M. M. et al. A multispectroscopic study of 3d orbitals in cobalt carboxylates: the high sensitivity of 2p3d resonant X-ray emission spectroscopy to the ligand field. *Angew. Chem. Int. Ed.* **52**, 1170–1174 (2012).
76. Ishihara, T., Tokushima, T., Horikawa, Y., Kato, M. & Yagi, I. Development of a spectro-electrochemical cell for soft X-ray photon-in photon-out spectroscopy. *Rev. Sci. Instrum.* **88**, 104101 (2017).
77. Chang, K. C. et al. in *In-situ Spectroscopic Studies of Adsorption at the Electrode and Electrocatalysis* (eds Sun, S.-G., Christensen, P. A. & Wieckowski, A.) 383–407 (Elsevier Science, New York, 2007).
78. Gul, S. et al. Simultaneous detection of electronic structure changes from two elements of a bifunctional catalyst using wavelength-dispersive X-ray emission spectroscopy and *in situ* electrochemistry. *Phys. Chem. Chem. Phys.* **17**, 8901–8912 (2015).
Demonstration of the feasibility of operando XES in tracking the chemical state of multi-component electrocatalysts during the oxygen evolution reaction.
79. Liu, Y., Barbour, A., Komanicky, V. & You, H. X-ray crystal truncation rod studies of surface oxidation and reduction on Pt(111). *J. Phys. Chem. C* **120**, 16174–16178 (2016).
80. Bouldin, C. E. et al. Diffraction anomalous fine structure: XAFS with virtual photoelectrons. *Jpn J. Appl. Phys.* **32**, 198 (1993).
81. Kawaguchi, T. et al. Roles of transition metals interchanging with lithium in electrode materials. *Phys. Chem. Chem. Phys.* **17**, 14064–14070 (2015).
82. He, J., Johnson, N. J. J., Huang, A. & Berlinguette, C. P. Electrocatalytic alloys for CO_2 reduction. *ChemSusChem* **11**, 48–57 (2018).
83. Mehdi, B. L. et al. Observation and quantification of nanoscale processes in lithium batteries by operando electrochemical (S)TEM. *Nano Lett.* **15**, 2168–2173 (2015).
84. Hodnik, N., Dehm, G. & Mayrhofer, K. J. J. Importance and challenges of electrochemical in situ liquid cell electron microscopy for energy conversion research. *Acc. Chem. Res.* **49**, 2015–2022 (2016).
85. Mierwaldt, D. et al. Environmental TEM investigation of electrochemical stability of perovskite and ruddlesden–popper type manganite oxygen evolution catalysts. *Adv. Sustain. Syst.* **1**, 1700109 (2017).

86. Mildner, S. et al. Environmental TEM study of electron beam induced electrochemistry of $Pr_{0.64}Ca_{0.36}MnO_3$ catalysts for oxygen evolution. *J. Phys. Chem. C* **119**, 5301–5310 (2015).
87. Yu, Y. et al. Three-dimensional tracking and visualization of hundreds of Pt–Co fuel cell nanocatalysts during electrochemical aging. *Nano Lett.* **12**, 4417–4423 (2012).
88. Zhang, D. et al. An *in situ* TEM study of the surface oxidation of palladium nanocrystals assisted by electron irradiation. *Nanoscale* **9**, 6327–6333 (2017).
89. Mancera, L. A., Behm, R. J. & Groβ, A. Structure and local reactivity of PdAg/Pd(111) surface alloys. *Phys. Chem. Chem. Phys.* **15**, 1497–1508 (2013).
90. Ustarroz, J. et al. Electrodeposition of highly porous Pt nanoparticles studied by quantitative 3D electron tomography: influence of growth mechanisms and potential cycling on the active surface area. *ACS Appl. Mater. Interfaces* **9**, 16168–16177 (2017).
91. Binnig, G., Rohrer, H., Gerber, C. & Weibel, E. Surface studies by scanning tunneling microscopy. *Phys. Rev. Lett.* **49**, 57–61 (1982).
92. Itaya, K. & Tomita, E. Scanning tunneling microscope for electrochemistry - a new concept for the *in situ* scanning tunneling microscope in electrolyte solutions. *Surf. Sci.* **201**, L507–L512 (1988).
93. Kim, Y.-G., Baricuatro, J. H., Javier, A., Gregoire, J. M. & Soriaga, M. P. The evolution of the polycrystalline copper surface, first to Cu(111) and then to Cu(100), at a fixed CO_2RR potential: a study by operando EC-STM. *Langmuir* **30**, 15053–15056 (2014).
94. Binnig, G., Quate, C. F. & Gerber, C. Atomic force microscope. *Phys. Rev. Lett.* **56**, 930–933 (1986).
95. Grosse, P. et al. Dynamic changes in the structure, chemical state and catalytic selectivity of Cu nanocubes during CO_2 electroreduction. *Angew. Chem. Int. Ed.* **57**, 6192–6197 (2018).
Dynamic morphological and chemical monitoring of Cu cubes during CO_2RR using operando EC-AFM and EXAFS. Roughening, loss of (100) facets and loss of Cu atoms from edge and corner sites, and the reduction of CuO_x species were observed, concommitant with reduced CO_2RR activity.
96. Nellist, M. R. et al. Potential-sensing electrochemical atomic force microscopy for in operando analysis of water-splitting catalysts and interfaces. *Nat. Energy* **3**, 46–52 (2018).
97. Jung, C., Sánchez-Sánchez, C. M., Lin, C.-L., Rodríguez-López, J. & Bard, A. J. Electrocatalytic activity of Pd–Co bimetallic mixtures for formic acid oxidation studied by scanning electrochemical microscopy. *Anal. Chem.* **81**, 7003–7008 (2009).
98. Bard, A. J., Fan, F. R. F., Kwak, J. & Lev, O. Scanning electrochemical microscopy. Introduction and principles. *Anal. Chem.* **61**, 132–138 (1989).
99. Lucas, M. & Boily, J.-F. Mapping electrochemical heterogeneity at iron oxide surfaces: a local electrochemical impedance study. *Langmuir* **31**, 13618–13624 (2015).
100. Sreekanth, N. & Phani, K. L. Selective reduction of CO_2 to formate through bicarbonate reduction on metal electrodes: new insights gained from SG/TC mode of SECM. *Chem. Commun.* **50**, 11143–11146 (2014).
101. Mariano, R. G., McKelvey, K., White, H. S. & Kanan, M. W. Selective increase in CO_2 electroreduction activity at grain-boundary surface terminations. *Science* **358**, 1187–1192 (2017).
The initial experimental demonstration of heightened CO_2RR activity at the grain boundary using SECM, as corroborated by electron backscattering diffraction (EBSD) grain mapping.
102. Kai, T., Zhou, M., Duan, Z., Henkelman, G. A. & Bard, A. J. Detection of $CO_2^{\bullet-}$ in the electrochemical reduction of carbon dioxide in *N*,*N*-dimethylformamide by scanning electrochemical microscopy. *J. Am. Chem. Soc.* **139**, 18552–18557 (2017).
Detection of CO_2 radical on Au substrate using SECM based on Hg/Pt ultra micro electrode. This is probably the initial experimental observation of CO_2 radical, which is extremely challenging due to the short lifetime of CO_2 radical and its reactivity with proton donors.
103. Lertanantawong, B. et al. Study of the underlying electrochemistry of polycrystalline gold electrodes in aqueous solution and electrocatalysis by large amplitude fourier transformed alternating current voltammetry. *Langmuir* **24**, 2856–2868 (2008).
104. Zhang, J., Guo, S.-X., Bond, A. M. & Marken, F. Large-amplitude Fourier transformed high-harmonic alternating current cyclic voltammetry: kinetic discrimination of interfering faradaic processes at glassy carbon and at boron-doped diamond electrodes. *Anal. Chem.* **76**, 3619–3629 (2004).
105. Guo, S. X., MacFarlane, D. R. & Zhang, J. Bioinspired electrocatalytic CO_2 reduction by bovine serum albumin-capped silver nanoclusters mediated by $[\alpha\text{-}SiW_{12}O_{40}]^{4-}$. *ChemSusChem* **9**, 80–87 (2016).
106. Zhang, Y. et al. Direct detection of electron transfer reactions underpinning the tin-catalyzed electrochemical reduction of CO_2 using Fourier-transformed ac voltammetry. *ACS Catal.* **7**, 4846–4853 (2017).
107. Liu, M. et al. Enhanced electrocatalytic CO_2 reduction via field-induced reagent concentration. *Nature* **537**, 382–386 (2016).
This work exploits the presence of charged reactant and intermediates, and demonstrates that CO_2RR activity can be enhanced by altering the local concentration of reactant due to the effect of electric field concentration on sharp tipped surfaces.
108. Huang, S. et al. Molecular selectivity of graphene-enhanced raman scattering. *Nano Lett.* **15**, 2892–2901 (2015).
109. Rehn, S. M. & Jones, M. R. New strategies for probing energy systems with in situ liquid-phase transmission electron microscopy. *ACS Energy Lett.* **3**, 1269–1278 (2018).
110. Schneider, N. M. et al. Electron–water interactions and implications for liquid cell electron microscopy. *J. Phys. Chem. C* **118**, 22373–22382 (2014).
111. Wu, J. et al. A metal-free electrocatalyst for carbon dioxide reduction to multi-carbon hydrocarbons and oxygenates. *Nat. Commun.* **7**, 13869 (2016).
112. Ma, X., Li, Z., Achenie, L. E. K. & Xin, H. Machine-learning-augmented chemisorption model for CO_2 electroreduction catalyst screening. *J. Phys. Chem. Lett.* **6**, 3528–3533 (2015).
113. Ulissi, Z. W. et al. Machine-learning methods enable exhaustive searches for active bimetallic facets and reveal active site motifs for CO_2 reduction. *ACS Catal.* **7**, 6600–6608 (2017).
114. de Groot, F. High-resolution X-ray emission and x-ray absorption spectroscopy. *Chem. Rev.* **101**, 1779–1808 (2001).
115. Artrith, N. & Kolpak, A. M. Understanding the composition and activity of electrocatalytic nanoalloys in aqueous solvents: a combination of dft and accurate neural network potentials. *Nano Lett.* **14**, 2670–2676 (2014).
116. Handoko, A. D. et al. Elucidation of thermally induced internal porosity in zinc oxide nanorods. *Nano Res.* **11**, 2412–2423 (2018).
117. Zaera, F. Infrared absorption spectroscopy of adsorbed CO: new applications in nanocatalysis for an old approach. *ChemCatChem* **4**, 1525–1533 (2012).
118. Fahrenkrug, E., Alsem, D. H., Salmon, N. & Maldonado, S. Electrochemical measurements in in situ TEM experiments. *J. Electrochem. Soc.* **164**, H358–H364 (2017).

Acknowledgements

This work was supported by the Institute of Materials Research and Engineering, A*STAR (IMRE/17-1R1211) and the National University of Singapore (R-143-000-A08-114).

Competing interests

The authors declare no competing interests.

Additional information

Supplementary information is available for this paper at https://doi.org/10.1038/s41929-018-0182-6.

Reprints and permissions information is available at www.nature.com/reprints.

Correspondence should be addressed to Z.W.S.

Publisher's note: Springer Nature remains neutral with regard to jurisdictional claims in published maps and institutional affiliations.